Summary

The chronological flow patterns around an airfoil that was oscillating in pitch with a relatively small amplitude were investigated using a smoke wire technique.

The unsteady separation observed in the present experiment was seen to be accomplished as the front of the reversed flow region reached its uppermost position. The separation did not necessarily take place when the instantaneous angle of attack α reached its maximum value. The instantaneous angle of attack at which the separation took place was seen to depend on the reduced frequency K. For flows with a larger K, the specific event of separation occurred at a larger phase angle ωt.

References

[1]Johnson, W. and Ham, N. D., "On the Mechanism of Dynamic Stall," *Journal of the American Helicopter Society*, Vol. 17, Oct. 1972, pp. 36–45.

[2]McCroskey, W. J., Carr, L. W., and McAlister, K. W., "Dynamic Stall Experiments on Oscillating Airfoils," *AIAA Journal*, Vol. 14, Jan. 1976, pp. 57–63.

[3]McAlister, K. W. and Carr, L. W., "Water Tunnel Visualizations of Dynamic Stall," *ASME Transactions, Series I—Journal of Fluids Engineering*, Vol. 101, Sept. 1979, pp. 376–380.

[4]Sears, W. R. and Telionis, D. P., "Boundary-Layer Separation in Unsteady Flow," *SIAM Journal on Applied Mathematics*, Vol. 28, Jan. 1975, pp. 215–235.

[5]Koromilas, C. A. and Telionis, D. P., "Unsteady Laminar Separation: an Experimental Study," *Journal of Fluid Mechanics*, Vol. 97, 1980, pp. 347–384.

[6]Park, S. O. and Kim, J. S., "Wake Measurements of an Oscillating Airfoil," *Proceedings of the International Symposium on Refined Flow Modelling and Turbulence Measurements*, Univ. of Iowa, Iowa City, IA, 1985, pp. D16-1–D16-10.

[7]Telionis, D. P., *Unsteady Viscous Flows*, Springer-Verlag, New York, 1981.

[8]Mehta, U. B. and Lavan, Z., "Starting Vortex, Separation Bubbles and Stall: a Numerical Study of Laminar Unsteady Flow around an Airfoil," *Journal of Fluid Mechanics*, Vol. 67, Pt. 2, 1975, pp. 227–256.

Viscous Effects on the Resonance of a Slotted Wind Tunnel Using Finite Elements

In Lee*

Stanford University, Stanford, California

Nomenclature

a_0 = speed of sound of fluid medium
a_e = effective speed of sound, $a_0\sqrt{1-M^2}$
h = half-width of slot
i = $\sqrt{-1}$
k = reduced frequency, $\omega h/a_0$
l = tunnel wall thickness
m = $M/1-M^2$
M = freestream Mach number
p = perturbation pressure
p_s = mean pressure
p^* = nondimensional perturbation pressure, p/p_s
s = shear wave number, $h\sqrt{\rho_s\omega/\mu}$
u = nondimensional velocity in $\bar{x}$ direction (Fig. 2)
$\bar{u}$ = velocity component in $\bar{x}$ direction (Fig. 2)
v = nondimensional velocity in $\bar{y}$ direction (Fig. 2)
w = nondimensional velocity in z direction (Fig. 2)
γ = ratio of specific heat
λ = eigenvalue
μ = viscosity coefficient of fluid
ρ = density, $\rho_s(1+\rho^*)$
ρ_s = density in undisturbed stream
ρ^* = nondimensional perturbation density
ω = angular frequency

Received May 26, 1987; revision received Feb. 22, 1988.

*Graduate Student, Department of Aeronautics and Astronautics; currently Assistant Professor at Department of Mechanical Engineering, Korea Advanced Institute of Science and Technology. Member AIAA.

I. Introduction

MODEL flutter and oscillatory airload measurements will be affected by coupling with an acoustic vibration mode when the model frequency is near a tunnel resonance frequency. Widmayer, Clevenson, and Leadbetter[1] conducted some experiments to measure the oscillatory aerodynamic forces and moments acting on a rectangular wing. The test results were in considerable error near the tunnel resonant frequency. Therefore, we want to predict the wind-tunnel resonant frequency accurately. Davis and Moore[2] and Acum[3] have obtained the resonance frequencies for a rectangular cross section. Lee[4] has obtained the resonance frequencies for an arbitrarily shaped cross section by using finite elements. These previous investigators have obtained the resonance frequencies without considering viscosity effects in the slot.

The effects of viscosity increase when the slot width becomes small. Many wind tunnels have a very small slot open area ratio (0–5%). When the slot width becomes small, wave propagation through the slot will be affected by the slot boundary layer. Tijdeman[5] has studied the propagation of sound waves in cylindrical tubes both analytically and numerically. The velocity-pressure ratio that is obtained by extending Tijdeman's approach to the slot is used as a boundary condition on the slot.

A finite-element treatment of the damping problem was given recently. Craggs[6] considered a damped acoustic system to study the performance of a muffler by the finite-element method. Kagawa et al.[7] considered an axisymmetric acoustic transmission with boundaries of acoustic impedance. Joppa and Fyfe[8] studied the impedance properties of arbitrarily shaped cavities with dissipative boundaries.

We will confine our concern to the wind tunnel that does not have a plenum chamber to simplify the problem, and we will discuss the case in which the slot width is very small to consider viscosity effects.

II. Governing Equation and Boundary Conditions

For a test section of a wind tunnel shown in Fig. 1, the following governing equation can be obtained from Ref. 4:

$$p_{xx} + p_{yy} + (\omega/a_e)^2 p = 0 \tag{1}$$

The boundary condition on the solid wall is given as

$$\frac{\partial p}{\partial n} = 0 \tag{2}$$

The boundary condition on the slot can be derived from the following linearized momentum equation:

$$\left(\frac{\partial}{\partial t} + U_\infty \frac{\partial}{\partial z}\right) u_n = -\frac{1}{\rho}\frac{\partial p}{\partial n} \tag{3}$$

where n is in the direction of the outward normal. For a narrow slot, the velocity component in the z direction inside a slot is very small ($U_\infty \approx 0$). Then, for a sinusoidal motion, we get

$$\frac{\partial p}{\partial n} = -i\rho\omega A p \tag{4}$$

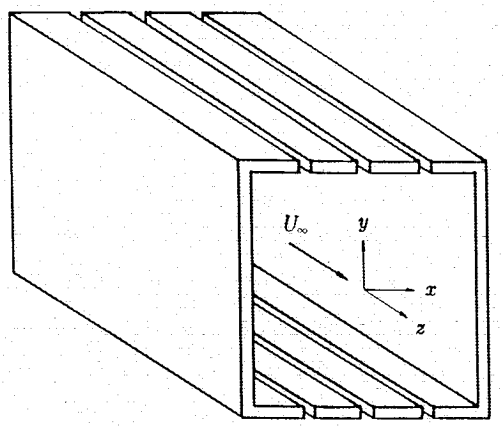

Fig. 1 Rectangular tunnel with slotted roof and floor.

where

$$A = u_n/p \tag{5}$$

where u_n is the normal velocity on the slot surface. Pressure, angular frequency, and A are complex quantities because we are considering a dissipative system.

III. Finite-Element Formulation

In this section, we consider the system with dissipation. Gladwell[9] gave a variational approach for studying damped vibration problems. The main idea is to consider an adjoint system that gains the energy the original dissipative system loses. In this way, the total energy is conserved, and we can have an invariant Lagrangian function.

Let us assume that pressure p of the real system and the pressure q of the adjoint system as

$$p = Pe^{i\omega t} \tag{6}$$

$$q = Qe^{i\omega t} \tag{7}$$

where P and Q are complex amplitudes and ω is a complex value. Then, the suitable functional for the test section with dissipation on the boundary is

$$F = \frac{1}{4\rho\omega^2}\int_V (\nabla P\cdot\nabla\bar{Q} + \nabla\bar{P}\cdot\nabla Q)\,dv - \frac{1}{4\rho a_e^2}\int_V (P\bar{Q} + \bar{P}Q)\,dv + \frac{i}{4\omega}\int_S (AP\bar{Q} - \bar{A}\bar{P}Q)\,dS \tag{8}$$

where A is the ratio of the normal velocity and the pressure on the open boundary, and an overbar indicates the complex conjugate. The sound pressure is a complex quantity for a system with dissipation.

The solution of the governing equations subjected to the boundary conditions can be replaced by an equivalent variational principle ($\delta F = 0$). Within each element, the pressure is approximated by a shape function.

$$P = [N]_i\{P\}_i \tag{9}$$

$$Q = [N]_i\{Q\}_i \tag{10}$$

For each element, the required functional can be obtained by substituting Eqs. (9) and (10) into Eq. (8). If we assemble all the elements, the functional F for the whole system is given as

$$F = \frac{1}{4\rho\omega^2}(\{P\}^T[M]\{\bar{Q}\} + \{\bar{P}\}^T[M]\{Q\}) - \frac{1}{4\rho a_e^2}(\{P\}^T[K]\{\bar{Q}\} + \{\bar{P}\}^T[K]\{Q\}) + \frac{i}{4\omega}(A\{P\}^T[C]\{\bar{Q}\} - \bar{A}\{\bar{P}\}^T[C]\{Q\}) \tag{11}$$

where $[M]$ and $[K]$ are the square symmetric mass and stiffness matrices for the whole system, respectively. The matrices $[M]$, $[K]$, and $[C]$ are defined as

$$[M] = \sum_i \int_{v_i} [B]^T[B]\,dv \tag{12}$$

$$[B] = \begin{Bmatrix} \frac{\partial}{\partial x} \\ \frac{\partial}{\partial y} \\ \frac{\partial}{\partial z} \end{Bmatrix} \lfloor N \rfloor_i \tag{13}$$

$$[K] = \sum_i \int_{v_i} \lfloor N \rfloor_i^T \lfloor N \rfloor_i\,dv \tag{14}$$

$$[C] = \sum_i \int_s \lfloor N \rfloor_i^T \lfloor N \rfloor_i\,dS \tag{15}$$

The first variation of Eq. (11), with respect to $\{\bar{Q}\}$, gives

$$[M]\{P\} - (\omega^2/a_e^2)[K]\{P\} + i\rho\omega A[C]\{P\} = 0 \tag{16}$$

Considering sinusoidal motion, Eq. (6), we can write Eq. (16) as

$$[K]\{\ddot{p}\} + \rho a_e^2 A[C]\{\dot{p}\} + a_e^2[M]\{p\} = 0 \tag{17}$$

Let us consider the following auxiliary equation:

$$[I]\{\dot{p}\} = [I]\{\dot{p}\} \tag{18}$$

Let us rewrite the pressure defined in Eq. (6) in the following form:

$$p = Pe^{\lambda t} \tag{19}$$

where $\lambda = i\omega$. Then, the two previous equations become an eigenvalue equation:

$$\begin{bmatrix} 0 & I \\ -a_e^2M & -\rho a_e^2AC \end{bmatrix}\begin{Bmatrix} p \\ \dot{p} \end{Bmatrix} - \lambda\begin{bmatrix} I & 0 \\ 0 & K \end{bmatrix}\begin{Bmatrix} p \\ \dot{p} \end{Bmatrix} = \begin{Bmatrix} 0 \\ 0 \end{Bmatrix} \tag{20}$$

An equation similar to Eq. (20) can be obtained for the adjoint system whose pressure is Q. However, we will use Eq. (20) because we are interested in the real system.

IV. Boundary Conditions at Slot

To determine the boundary condition at the slot surface, the propagation of pressure waves in the slot has to be considered.

Figure 2 shows the coordinate system of the slot. The boundary condition at the slot can be obtained by extending Tijdeman's approach[5] to the slot.

When the slot width is small, compared to the wavelength, and the velocity component v is small, compared to the veloci-

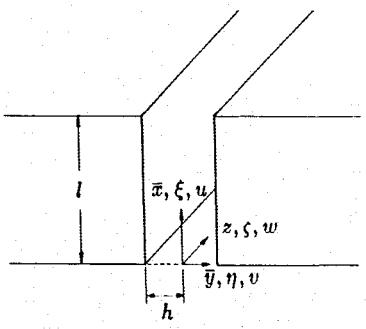

Fig. 2 Transonic slot.

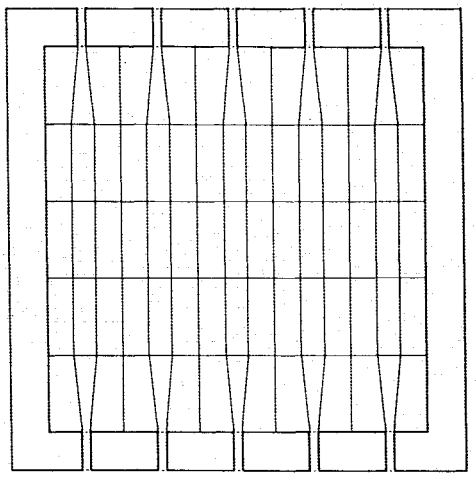

Fig. 3 Finite-element mesh for the rectangular wind tunnel with five slots each on roof and floor.

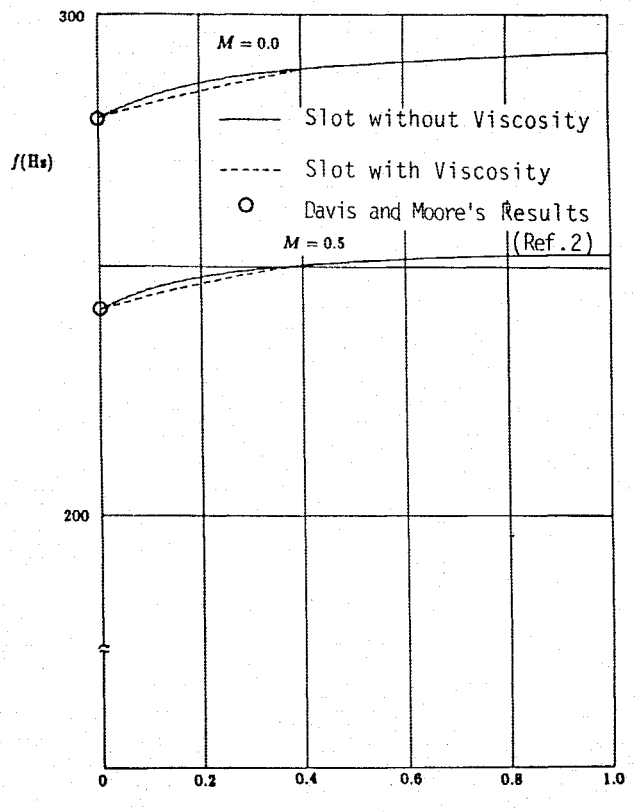

Fig. 4 Viscosity effect on resonant frequency of rectangular tunnel.

ties u and w, then we can assume the following inequalities:

$$(\omega h/a_0) \ll 1 \tag{21}$$

$$(v/u) \ll 1 \tag{22}$$

$$(v/w) \ll 1 \tag{23}$$

Given these assumptions, the Navier-Stokes equations for sinusoidal motion become

$$iu = -\frac{1}{\gamma}\frac{\partial p^*}{\partial \xi} + \frac{1}{s^2}\frac{\partial^2 u}{\partial \eta^2} \tag{24}$$

$$0 = -\frac{1}{\gamma}\frac{\partial p^*}{\partial \eta} \tag{25}$$

$$iw = -\frac{im}{\gamma}p^* + \frac{1}{s^2}\frac{\partial^2 w}{\partial \eta^2} \tag{26}$$

and the equation of continuity becomes

$$ik\rho^* = -\left(k\frac{\partial u}{\partial \xi} + \frac{\partial v}{\partial \eta}\right) \tag{27}$$

When the slot width is very much reduced, the conduction of heat from the center of the slot to the wall becomes more and more free, and the expansions and rarefactions take place isothermally. Therefore, we can assume that the inside of the slot is isothermal. Then, the equation of state for an ideal gas becomes

$$p^* = \rho^* \tag{28}$$

After applying no slip boundary conditions at the slot wall, we can get the following relation on the slot:

$$A = \frac{\bar{u}}{p} = -\frac{i\Gamma}{\rho_s a_0}\left[1 - \frac{\sinh(\sqrt{i}\,hs)}{\sqrt{i}\,hs\cosh(\sqrt{i}\,s)}\right]\coth\left(\frac{\omega l\Gamma}{a_0}\right) \tag{29}$$

where

$$\Gamma = \sqrt{(\gamma\sqrt{i}\,s)/(\tanh(\sqrt{i}\,s) - \sqrt{i}\,s)} \tag{30}$$

Discussion

Let us consider the rectangular cross section. The finite-element mesh is given in Fig. 3. The height and width of the wind tunnel are 2 ft each. There are five slots each on the roof and floor. The slot length is 0.1 ft. The standard atmospheric values were used for the calculation.

The results for the viscosity effect in the slot are plotted in Fig. 4. Circular symbols are the results of Davis and Moore's[2] results for the slot-closed condition.

The solid curves represent the resonant frequency for the slot without considering the viscosity in the slot. These curves are obtained by applying the boundary condition $p = 0$ at the outside slot end. The dotted curves represent the viscosity effects in the slot. As the slot width increases, the viscosity effect decreases. However, when the slot width approaches zero, the viscosity effect also decreases. In other words, when the slot width approaches zero, the boundary condition at the slot is close to the solid boundary condition. The viscosity effect becomes large when the slot open ratio is less than 0.5%. Although viscosity effects on the tunnel resonance are small in this case, the viscosity effects will increase significantly for wind tunnels with many slots or holes on the test-section wall.

Acknowledgment

This research was performed under NASA Grant NGL-05-020-243. The author wishes to express his appreciation to Professor H. Ashley for his valuable discussions.

References

[1]Widmayer, E., Clevenson, S. A., and Leadbetter, S. A., "Some Measurements of Aerodynamic Forces and Moments at Subsonic Speeds on a Rectangular Wing of Aspect Ratio 2 Oscillating About the Midchord," NASA TN 4240, 1958.

[2]Davis, D. D. and Moore, D., "Analytical Study of Blockage and Lift-Interference Corrections for Slotted Tunnels Obtained by the Substitution of an Equivalent Homogeneous Boundary for the Discrete Slots," NASA Research Memo L53E07b, June 1953.

[3]Acum, W. E. A., "A Simplified Approach to the Phenomenon of Wind Tunnel Resonance," Aeronautical Research Council Reports and Memoranda No. 3371, 1962.

[4]Lee, I., "Resonance Prediction for Slotted Wind Tunnel by the Finite Element Method," AIAA Paper 86-0898, May 1986.

[5]Tijdeman, H., "On the Propagation of Sound Waves in Cylindrical Tubes," *Journal of Sound and Vibration*, Vol. 39, March 1975, pp. 1-33.

[6]Craggs, A., "A Finite Element Method for Damped Acoustic Systems: An Application to Evaluate the Performance of Reactive Mufflers," *Journal of Sound and Vibration*, Vol. 48, Oct. 1976, pp. 377-392.

[7]Kagawa, Y., Yamabuchi, T., and Mori, A., "Finite Element Simulation of an Axisymmetric Acoustic Transmission System with a Sound Absorbing Wall," *Journal of Sound and Vibration*, Vol. 53, Aug. 1977, pp. 357-374.

[8]Joppa, P. D. and Fyfe, I. M., "A Finite Element Analysis of the Impedance Properties of Irregular Shaped Cavities with Absorptive Boundaries," *Journal of Sound and Vibration*, Vol. 56, Jan. 1978, pp. 61-69.

[9]Gladwell, G. M. L., "A Variational Formulation of Damped Acousto-Structural Vibration Problems," *Journal of Sound and Vibration*, Vol. 4, Sept. 1966, pp. 172-186.

Iterative Methods for Design Sensitivity Analysis

B. G. Yoon* and A. D. Belegundu†
Pennsylvania State University, University Park, Pennsylvania

Introduction

ITERATIVE methods are presented for obtaining design sensitivity coefficients (or derivatives) of implicit functions. Design derivatives are important not only in gradient-based optimization codes, but also for examining tradeoffs, system identification, and probabilistic design, to name a few. Iterative methods are presented for both the algebraic and eigenvalue problems; stress, eigenvalue, and eigenvector derivatives are considered. The iterative approaches provide approximate derivatives. They are very simple to implement in a program, even for complex structural response. Iterative methods for sensitivity, for a class of structural problems, were suggested in Ref. 1. General papers on reanalysis schemes may be found in Refs. 2 and 3.

In the next section, iterative methods for sensitivity of displacement and stress are developed. Following this, eigenvalue and eigenvector sensitivity is considered.

Displacement and Stress Sensitivity

The problem of obtaining design derivatives of displacements and stresses, for a finite-element model of the structure, is considered. Consider a function $g = g(b, z)$. This represents a stress constraint, with $\boldsymbol{b} = (k \times 1)$ design vector and $\boldsymbol{z} = (n \times 1)$ displacement vector, which is obtained from the finite-element equations $\boldsymbol{K}(\boldsymbol{b})\ \boldsymbol{z} = \boldsymbol{F}(\boldsymbol{b})$, where $\boldsymbol{K}$ is an $(n \times n)$ structural stiffness matrix, and $\boldsymbol{F}$ is an $(n \times 1)$ nodal load vector. Let $\boldsymbol{b}^0$ be the current design. At this stage, the analysis has been completed. Thus, the decomposed $\boldsymbol{K}(\boldsymbol{b}^0)$ and $\boldsymbol{z}^0$ are known. The derivative of the function g with respect to the ith design variable is given by

$$\frac{\mathrm{d}g}{\mathrm{d}b_i} = \frac{\partial g}{\partial b_i} + \frac{\partial g}{\partial \boldsymbol{z}} \cdot \frac{\mathrm{d}\boldsymbol{z}}{\mathrm{d}b_i} \tag{1}$$

The partial derivatives $\partial g/\partial \boldsymbol{b}$ and $\partial g/\partial \boldsymbol{z}$ are readily available using the finite-element relations. The problem, therefore, is to compute the displacement sensitivity $\mathrm{d}\boldsymbol{z}/\mathrm{d}\boldsymbol{b}$. An iterative approach for computing this is now given.

Corresponding to the ith design variable, let the perturbed design vector $\boldsymbol{b}^\epsilon$ be defined as

$$\boldsymbol{b}^\epsilon = (b_1^0, b_2^0, \ldots, b_i^0 + \epsilon, \ldots, b_k^0)^T \tag{2}$$

The perturbation ϵ is relatively small, and a value of 1% of b_i is suggested. The problem is to find $\boldsymbol{z}^\epsilon$, the solution of

$$\boldsymbol{K}(\boldsymbol{b}^\epsilon)\ \boldsymbol{z}^\epsilon = \boldsymbol{F}(\boldsymbol{b}^\epsilon) \tag{3}$$

using the decomposed $\boldsymbol{K}(\boldsymbol{b}^0)$ and $\boldsymbol{z}^0$. A modified version of the residual-correction scheme given in Ref. 3 is given below.

Algorithm 1 (Displacement and Stress Sensitivity)

Step 0: Set $j = 0$. Choose the perturbation ϵ and the error tolerance Δ. Define $\boldsymbol{b}^\epsilon$ as in Eq. (2).

Step 1: Calculate the residual $\boldsymbol{r}^j$ from

$$\boldsymbol{r}^j = \boldsymbol{K}(\boldsymbol{b}^\epsilon)\ \boldsymbol{z}^j - \boldsymbol{F}(\boldsymbol{b}^\epsilon) \tag{4}$$

Step 2: Solve for the correction $\boldsymbol{e}^j$ from

$$\boldsymbol{K}(\boldsymbol{b}^0)\ \boldsymbol{e}^j = -\boldsymbol{r}^j \tag{5}$$

Step 3: Update $\boldsymbol{z}^{j+1} = \boldsymbol{z}^j + \boldsymbol{e}^j$

Step 4: Check the convergence criterion

$$||\boldsymbol{z}^{j+1} - \boldsymbol{z}^j|| \le \Delta \tag{6}$$

If satisfied, then set $\boldsymbol{z}^\epsilon = \boldsymbol{z}^{j+1}$, and compute the displacement sensitivity as

$$\frac{\mathrm{d}\boldsymbol{z}}{\mathrm{d}b_i} \approx \frac{\boldsymbol{z}^\epsilon - \boldsymbol{z}^0}{\epsilon} \tag{7}$$

The stress sensitivity can be recovered from Eq. (1). Otherwise, set $j = j + 1$ and re-execute steps 1-4.

Numerical results and comparison with the exact and semi-analytical methods discussed in the literature are presented subsequently. Theoretically, it can be shown that the above scheme will converge provided[3]

$$r_o[\boldsymbol{I} - \boldsymbol{K}^{-1}(\boldsymbol{b}^0)\ \boldsymbol{K}(\boldsymbol{b}^\epsilon)] < 1 \tag{8}$$

where $r_o(\boldsymbol{A})$ = spectral radius of the matrix $\boldsymbol{A}$, which is the maximum size of the eigenvalues of $\boldsymbol{A}$. In the problem considered here, $\boldsymbol{K}(\boldsymbol{b}^0)$ and $\boldsymbol{K}(\boldsymbol{b}^\epsilon)$ are roughly equal because ϵ is small, and Eq. (8) can generally be expected to hold.

Eigenvalue and Eigenvector Sensitivity

Eigenvalue sensitivity is useful when resonant frequencies or critical buckling loads need to be restricted. Exact analytical expressions for eigenvalue sensitivity can be readily derived for the case of nonrepeated roots.[4] The problem of obtaining eigenvector sensitivity, on the other hand, is more complicated

Received Jan. 25, 1988; revision received July 20, 1988.

*Graduate Student, Department of Mechanical Engineering.

†Assistant Professor, Department of Mechanical Engineering. Member AIAA.